

LIMITS ON MASS AND RADIUS FOR THE MS-PERIOD X-RAY PULSAR SAX J1808.4-3658

DENIS A. LEAHY¹, SHARON M. MORSINK^{2,3}, COIRE CADEAU²

Submitted to ApJ Letters on March 8, 2007

ABSTRACT

We present an analysis of the light curves of SAX J1808.4-3658 during its 1998 and 2002 outbursts. We assume a hot spot model where the X-rays are originate from the surface of the neutron star. We obtain 80%, 90%, 2σ and 3σ limits on the mass and radius of SAX J1808.4-3658, which suggest a soft equation of state. At the 3σ level, the radius must satisfy $R < 11.9$ km which rules out very stiff equations of state. At the 2σ level, the radius must satisfy $R < 11.6$ km, ruling out equations of state with more moderate stiffness.

Subject headings: stars: neutron — stars: rotation — X-rays: binaries — relativity — pulsars: individual: SAX J1808.4-3658

1. INTRODUCTION

The discovery of 2.5 ms pulsations originating from SAX J1808.4-3658 (Wijnands & van der Klis 1998) provides strong evidence that the neutron stars in low mass X-ray binaries are the progenitors of the millisecond period pulsars. SAX J1808.4-3658 is now one of 7 known accreting ms X-ray pulsars (see Wijnands (2005) for a review of the properties of the first 6 pulsars of this type).

The pulsed X-rays observed during outburst are most likely produced from the energy released from accretion of plasma funnelled onto the neutron star's magnetic poles (see for example, Figure 12 of Gierliński et al (2002)). Spectral models (Gilfanov et al 1998; Gierliński et al 2002; Poutanen & Gierliński 2003) provide strong evidence that the X-rays correspond to blackbody emission from a spot on the star which is then Compton scattered by electrons above the hot spot. Since, in this model, the pulsed light is emitted from the neutron star's surface (or from a region very close to the surface) the accreting ms X-ray pulsars are excellent targets for light curve fitting in order to constrain the neutron star equation of state. The X-ray light curve depends on the intrinsic properties of the emission (spot shape, size, location and emissivity) as well as the neutron star's macroscopic properties (mass, radius and spin). If tight enough constraints on the star's mass and radius can be made, it could be possible to constrain the equation of state of supernuclear density material.

The first pulse shape analysis (Poutanen & Gierliński 2003) for SAX J1808.4-3658 provided interesting constraints on the neutron star's mass and radius. However, this analysis did not take into account two effects that are potentially important for rapidly rotating neutron stars: variable time delays due to light travel time across the star (Cadeau et al. 2005) and the oblate shape of the star (Cadeau et al. 2007). One of the motivations for the re-examination of the pulse shapes for SAX J1808.4-3658 is

to include these effects in the analysis. In addition, at the time that the paper by Poutanen & Gierliński (2003) was written, only data corresponding to the 1998 outburst was available. The pulse profile since recorded during the 2002 outburst (Papitto et al. 2005) shows a much stronger harmonic content than the 1998 outburst data. In this Letter we analyse both data sets and provide a new set of best fit models consistent with both data sets.

2. METHOD

Precise light curves were constructed by Papitto et al. (2005) (shown in their Figure 2) using data collected by RXTE during the 1998 and 2002 outbursts. In their analysis, they binned the X-ray flux from all energy channels into 64 bins per rotational period. The 1998 light curve is constructed from data collected on April 18 and 19 and is very close to sinusoidal. The 2002 light curve is constructed from data collected on October 17 (see Papitto et al. (2005) for more details). In our analysis, we use the light curves exactly as published by Papitto et al. (2005). The data has been reproduced in Figure 1.

Our modelling of the data follows a method similar to the Schwarzschild + Doppler (S+D) approximation described by Poutanen & Gierliński (2003). We now proceed to list the ways in which our analysis differs from the S+D method given by Poutanen & Gierliński (2003). (1) We include the variable time delays caused by photons taking different amounts of time to travel to the observer depending on the location of the emitting region on the star. (2) We include the oblate shape of the star using the Oblate Schwarzschild (OS) approximation. This approximation makes use of a simple empirical formula (Morsink et al 2007) describing the star's oblate shape based on two parameters, M/R and $\Omega^2 R^3/M$. The shape function is used to compute the true angle β between the normal to the surface and the initial photon direction. In the S+D approximation the solid angle subtended by a spot is proportional to $\cos\alpha$ where α is the angle between the radial direction and the photon's initial direction. In the OS approximation the $\cos\alpha$ dependence is replaced by $\cos\beta$. Light bending and time delays are computed using the Schwarzschild metric and Doppler effects are introduced in exactly the same manner as in the S+D approximation (Cadeau et al. 2007; Morsink et al 2007). (3) In our treatment of the data, all

¹ Department of Physics and Astronomy, University of Calgary, Calgary AB, T2N 1N4, Canada

² Department of Physics, University of Alberta, Edmonton, AB, T6G 2G7, Canada

³ On sabbatical at: Pacific Institute for Theoretical Physics, Department of Physics and Astronomy, University of British Columbia, 6224 Agricultural Road, Vancouver BC, V6T 1Z1, Canada

data from all energy channels is binned together into 64 timing bins per rotational period. Poutanen & Gierliński (2003) separated light in different energy ranges into separate light curves binned into 16 bins per rotational period. Thus our analysis provides better timing resolution while the analysis by Poutanen & Gierliński (2003) provides better energy resolution.

In our modelling we use a simplified spectral model that assumes that all of the received photons have been Compton scattered resulting in a power law spectrum and “fan” beaming of emission. In particular, we use an emissivity model of the form $I(\cos \beta_{em}) = 1 - a \cos \beta_{em}$ where the constant a is an adjustable parameter and β_{em} is the angle between the normal and the initial photon direction as measured in the star’s rest frame. We allow for spots of different sizes in our models, however it is beyond the scope of our models to allow for intensity variations across the spot or for complicated shapes. In all of our models the pulsed emission is assumed to originate from the surface of the star.

In our modelling we first choose a model which has fixed values of: the emissivity parameter a ; spot size; ratio of M/R as measured at the spot location; and spin frequency $\nu = 401$ Hz. After these parameters have been fixed, the following 8 parameters are allowed to vary: ϕ_1 , ϕ_2 , I_1 , I_2 , i , θ_1 , θ_2 and M . In our notation, the subscript “1” refers to the 1998 data while “2” refers to the 2002 data. The mass of the star M and the inclination angle i are restricted to have the same value for the fits to the 1998 and 2002 data. The phase constants ϕ_1 and ϕ_2 , intensities I_1 and I_2 and spot co-latitudes θ_1 and θ_2 are allowed to differ when modelling the two data streams. We do not make use of the most probable (Galloway & Cumming 2006) distance of 3.5 kpc to the source in our analysis. After values of these 8 parameters have been chosen, the χ^2 for this set of parameters is computed. The set of parameters that minimize χ^2 is then the best fit for the assumed choice of a , M/R and spot size. This results in a family of best fit models with different values of M/R .

3. RESULTS

In our first models we allow for 2 antipodal hot spots. However, the best fit models always converge to geometries where only one spot is visible. Hence we limit our models to single hot spots. In our models we are assuming that the main reason for the change in the light curves is that the location of the spot has changed, but that the size of the spot has not changed. In Table 1 we show how variation in spot size affects the fits. In this group of models the compactness ratio is fixed at $2M/R = 0.4$ and the emissivity constant is fixed at $a = 0.7$. (The results are similar for other choices of $2M/R$ and a .) Choosing an infinitesimal spot results in a poor fit. Allowing the source to have a large azimuthal angular size ($d\phi = 0.4$) does not significantly change the fit parameters or the quality of the fit. Allowing the spot to extend over a range of latitudes improves the quality of the fit and changes the values of the best fit parameters by a small amount. Although the fit improves as the range of allowed latitudes is increased, the spot size can’t be increased to arbitrarily large size: the best fit models always converge to models where the spots are close to the spin axis. If the extent in latitude is increased beyond 0.2

radians the spots run over the spin axis. For this reason we choose to keep the spot size fixed at this largest possible value for the rest of the models. We note that more complicated spot patterns have been predicted by MHD simulations of accretion (Kulkarni & Romanova 2005). However, since the degrees of freedom in our model is $128 - 8 = 120$, we are achieving a good statistical fit with our simple spot shapes. At the current level of accuracy in the data there is no need to consider more complicated spot shapes.

The assumed angular dependence of the emitted light could potentially affect the fits. The simple dependence (with $0 < a < 1$) that we assume is an approximation to the more detailed calculations (Sunyaev & Titarchuk 1985) of Comptonized radiation. In this range of emissivity parameters, we found that χ^2 is minimized near $a = 0.7$. In Table 2 we show a group of best fit models with $2M/R = 0.4$, $d\theta = 0.2$ and various values of a close to 0.7. It can be seen that small changes in a cause large changes in χ^2 but leave the best fit parameters (M , θ , etc.) virtually unchanged. (This result holds for other values of $2M/R$ and spot size.) We also experimented with other emissivity models but did not find a noticeable difference in the results. For the remaining models we keep the emissivity parameter fixed at $a = 0.7$.

In Table 3 we demonstrate the importance of including time delays and oblateness when modelling rapidly rotating neutron stars. In the three models shown in this table, the spot size, emissivity and compactness are kept at fixed values. In the first row we show the best fit parameters if the light curves are computed by omitting time delays and assuming a spherical star. The result in this case is a very large star. In the second row the best fit parameters for a model where time delays are included but the assumption of sphericity is kept, resulting in a star which is smaller by about 4 km. Including time delays and including the star’s oblateness further reduces the radius by another km. Clearly the inclusion of time delays and oblateness strongly affect the best fit results.

The best fit models are displayed in Table 4. For all models in this table the spot width is fixed at $d\theta = 0.2$ and the emissivity parameter is fixed at $a = 0.7$. Each row in the table corresponds to a different fixed value of $2M/R$. All other parameters are kept free. The light curve corresponding to the $2M/R = 0.4$ model is plotted (with the data) in Figure 1.

Figure 2 shows the mass versus equatorial radius curves for stars rotating at 401 Hz for a number of EOS. (Note that the radii of these stars are about 10% larger than non-rotating stars with the same masses.) Contours of constant confidence levels corresponding to 80%, 90%, 95.4% (2σ) and 99.7% (3σ) for these fits are shown as dashed curves.

It can be seen from Figure 2 that soft EOS are favoured from this analysis. At the 99.7% confidence level our data only allow radii in the range $6.9 \text{ km} \leq R \leq 11.9 \text{ km}$ and masses in the range $0.75M_\odot \leq M \leq 1.56M_\odot$, excluding the stiffest equations of state, such as those including hyperons. At the 90% confidence level the neutron star’s radius is restricted to the range $8.6 \text{ km} \leq R \leq 11.4 \text{ km}$ and the mass to the range $0.85M_\odot \leq M \leq 1.42M_\odot$. At the 90% confidence level moderately stiff equations of state (such as APR Akmal et al. (1998) and some hybrid quark-hadron stars) are excluded.

Comparing our results with those of Poutanen & Gierliński (2003), it can be seen that our new results are more restrictive. At the 3σ confidence level, Poutanen & Gierliński (2003) found that $R < 15$ km, 3 km larger than our upper limit at the 3σ level. Similarly the smallest star allowed by Poutanen & Gierliński (2003) is 4.8 km, which is 2 km smaller than our smallest allowed radius.

Chakrabarty & Morgan (1998) note that the lack of deep X-ray eclipses restricts the inclination angle to be $i < 82^\circ$. The best fit results (shown in Table 4) are consistent with this requirement. Making use of the known mass function (Chakrabarty & Morgan 1998) and our best fit masses and inclination angles, the companion mass for all of the best fit solutions is $0.04M_\odot$, consistent with a brown dwarf as first proposed by Bildsten & Chakrabarty (2001).

4. DISCUSSION

Our results favour a soft EOS for SAX J1808.4-3658. In contrast, recent measurements of the quiescent flux from SAX J1808.4-3658 (Heinke et al 2007) suggest a stiff EOS due to the very low inferred luminosity. While the measurements by Heinke et al (2007) are quite robust, further exploration of cooling processes in quark and other soft EOS are probably required to truly rule out a soft EOS solely on the basis of observations during quiescence.

Our 90% confidence limits only allow soft EOS which (with one exception) have low maximum masses below $1.6M_\odot$. (The exception corresponds to quark star models with low bag constant, such as the Q140 EOS.) The model-independent mass measurement of $2.1M_\odot$ for PSR J0751+1807 (Nice et al. 2005) rules out these soft EOS. However, the 95% confidence limits (Nice et al. 2005) on PSR J0751+1807 allow for a mass of only $1.6M_\odot$. Our 99.7% confidence limits allow stiffer EOS (such as APR)

with maximum masses above $2.0M_\odot$, so there is not necessarily any conflict with the results of Nice et al. (2005).

Our results are consistent with a number of other EOS constraints derived for other neutron stars. A pulse shape analysis for the slowly rotating X-ray pulsar Her X-1 (Leahy 2004) also favoured a softer EOS. The bounds on Her X-1 are more restrictive than ours in that all EOS allowed (at the 3σ level) by the Her X-1 analysis are also allowed by our analysis of SAX J1808.4-3658. The softest quark EOS allowed by our analysis is not allowed by the Her X-1 data.

An analysis of X-ray bursts originating from EXO 0748-676 by Özel (2006) predicts a stiff EOS at the 1σ confidence level. However at the 2σ confidence level the analysis allows softer EOS (see, for example Alford et al. (2006)) compatible with our results.

The fact that SAX J1808.4-3658 is an accreting neutron star and has a very rapid rotation rate suggests that it may have accreted a large amount of mass. However, it should be remembered that a high spin rate does not necessarily require a large accretion of mass. Cook et al. (1994) showed that it is possible to spin a $1.4M_\odot$ star up to 640 Hz by accreting as little as $0.1M_\odot$ if the EOS is soft. Smaller mass stars have lower moments of inertia and are easier to spin up, so it is plausible that our model with $M = 1.32M_\odot$ could have been born with a mass as high as $1.2M_\odot$, consistent with the masses of neutron stars in binary pulsar systems (Stairs 2004).

This research was supported by grants from NSERC. We thank Ingrid Stairs for helpful comments about the masses of radio pulsars. S. M. M. thanks the Pacific Institute for Theoretical Physics and the Department of Physics and Astronomy at the University of British Columbia for hospitality during her sabbatical.

REFERENCES

- Akmal, A., Pandharipande, V. R., & Ravenhall, D. G. 1998, Phys. Rev. C, 58, 1804
 Alford, M., Braby, M., Paris, M., & Reddy, S. 2005, ApJ 629, 969
 Alford, M., Blaschke, D., Drago, A., Klahn, T., Pagliara, G., & Schaffner-Bielich, J. 2006, astro-ph/0606524
 Arnett, W. D., & Bowers, R. L. 1977, ApJS, 33, 415
 Bildsten, L., & Chakrabarty, D. 2001, ApJ, 557, 292
 Cadeau, C., Leahy, D. A., & Morsink, S. M. 2005, ApJ, 618, 451
 Cadeau, C., Morsink, S. M., Leahy, D. A., & Campbell, S. S. 2007, ApJ, 654, 458
 Chakrabarty, D. & Morgan, E. H. 1998, Nature, 394, 346
 Cook, G. B., Shapiro, S. L., & Teukolsky, S. A. 1994, ApJ, 423, L117
 Galloway, D. K., & Cumming, A. 2006, ApJ, 652, 559
 Gierliński, M., Done, C., & Barret, D. 2002, MNRAS, 331, 141
 Gilfanov, M., Revnivtsev, M., Sunyaev, R., & Churazov, E. 1998, A&A, 338, L83
 Glendenning, G. K. 2000, *Compact Stars*, (Springer-Verlag, New York)
 Heinke, C. O., Jonker, P. G., Wijnands, R., & Taam, R. E. 2007, ApJ, to appear, astro-ph/0612232
 Kulkarni, A. K. & Romanova, M. M. 2005, ApJ, 633, 349
 Lackey, B. D., Nayyar, M., & Owen, B. J. 2006, Phys. Rev. D, 73, 024021
 Leahy, D. A. 2004, ApJ, 613, 517
 Morsink, S. M., Leahy, D. A., Cadeau, C. & Braga, J. 2007, ApJ, submitted, astro-ph/0703123
 Nice, D. J., Splaver, E. M., Stairs, I. H., Löhmer, O., Jessner, A., Kramer, M., & Cordes, J. M. 2005, ApJ, 634, 1242
 Özel, F. 2006, Nature, 441, 1115
 Papitto, A., Menna, M. T., Burderi, L., Di Salvo, T., D'Antona, F., & Robba, N. R. 2005, ApJ, 621, L113
 Poutanen, J. & Gierliński, M. 2003, MNRAS, 343, 1301
 Stairs, I. H. 2004, Science, 304, 547
 Sunyaev, R. A., & Titarchuk, L. G. 1985, A&A, 143, 374
 Wijnands, R. 2005, arXiv:astro-ph/0501264
 Wijnands, R., & van der Klis, M. 1998, Nature, 394, 344

TABLE 1
EFFECT OF SPOT SIZE

| Model ^a | Mass M_{\odot} | R ^b km | θ_1 | θ_2 | i | χ^2 ^c |
|----------------------|---------------------|------------------------|------------|------------|-------|-----------------------|
| Infinitesimal | 1.24 | 9.3 | 11.8° | 7.1° | 68.0° | 153.1 |
| $d\phi = 0.4$ rad | 1.21 | 9.0 | 12.4° | 7.5° | 67.5° | 152.0 |
| $d\theta = 0.1$ rad | 1.27 | 9.5 | 11.6° | 6.9° | 68.3° | 147.4 |
| $d\theta = 0.15$ rad | 1.29 | 9.7 | 11.3° | 6.7° | 68.5° | 139.9 |
| $d\theta = 0.2$ rad | 1.31 | 9.8 | 11.2° | 6.6° | 68.6° | 130.1 |

^a $2M/R = 0.4$ and $a = 0.7$ for all models.

^b Radius at the star's equator.

^c Degrees of freedom = $128 - 8$.

TABLE 2
EFFECT OF EMISSIVITY

| Model ^a | Mass M_{\odot} | R ^b km | θ_1 | θ_2 | i | χ^2 ^c |
|--------------------|---------------------|------------------------|------------|------------|-------|-----------------------|
| $a = 0.60$ | 1.33 | 10.0 | 10.4° | 6.8° | 62.3° | 196.3 |
| $a = 0.65$ | 1.33 | 10.0 | 10.8° | 6.8° | 65.4° | 153.1 |
| $a = 0.70$ | 1.32 | 9.9 | 11.1° | 6.6° | 68.7° | 130.1 |
| $a = 0.75$ | 1.32 | 9.9 | 10.9° | 6.9° | 71.9° | 138.6 |
| $a = 0.80$ | 1.32 | 9.9 | 10.9° | 6.9° | 74.9° | 159.3 |

^a Spot width is $d\theta = 0.2$ radians and $2M/R = 0.4$ for all models.

^b Radius at the star's equator.

^c Degrees of freedom = $128 - 8$.

TABLE 3
EFFECT OF CALCULATION METHOD

| Model ^a | Mass M_{\odot} | R ^b km | θ_1 | θ_2 | i | χ^2 ^c |
|-------------------------------|---------------------|------------------------|------------|------------|-------|-----------------------|
| Spherical, no TD ^d | 2.06 | 15.2 | 10.3° | 6.2° | 67.6° | 135.7 |
| Spherical, with TD | 1.50 | 11.0 | 9.7° | 5.8° | 68.4° | 129.5 |
| Oblate, with TD | 1.32 | 9.9 | 11.1° | 6.6° | 68.7° | 130.1 |

^a $d\theta = 0.2$ rad., $2M/R = 0.4$ and $a = 0.7$ for all models.

^b Radius at the star's equator.

^c Degrees of freedom = $128 - 8$.

^d TD = time delays

TABLE 4
BEST FIT MODELS ^a

| Mass M_{\odot} | R ^b km | $2M/R$ | θ_1 | θ_2 | i | χ^2 ^c |
|---------------------|------------------------|--------|------------|------------|-------|-----------------------|
| 1.40 | 7.5 | 0.55 | 13.1° | 7.8° | 80.3° | 135.1 |
| 1.41 | 8.4 | 0.50 | 12.2° | 7.2° | 75.8° | 132.9 |
| 1.37 | 9.1 | 0.45 | 11.7° | 6.9° | 71.8° | 131.4 |
| 1.32 | 9.9 | 0.40 | 11.1° | 6.6° | 68.7° | 130.1 |
| 1.21 | 10.4 | 0.35 | 11.0° | 6.6° | 65.5° | 129.8 |
| 1.07 | 10.8 | 0.30 | 11.0° | 6.6° | 62.7° | 130.5 |
| 0.91 | 11.1 | 0.25 | 10.9° | 6.6° | 60.8° | 130.9 |

^a Spot width is $d\theta = 0.2$ radians for all models.

^b Radius at the star's equator.

^c Degrees of freedom = $128 - 8$.

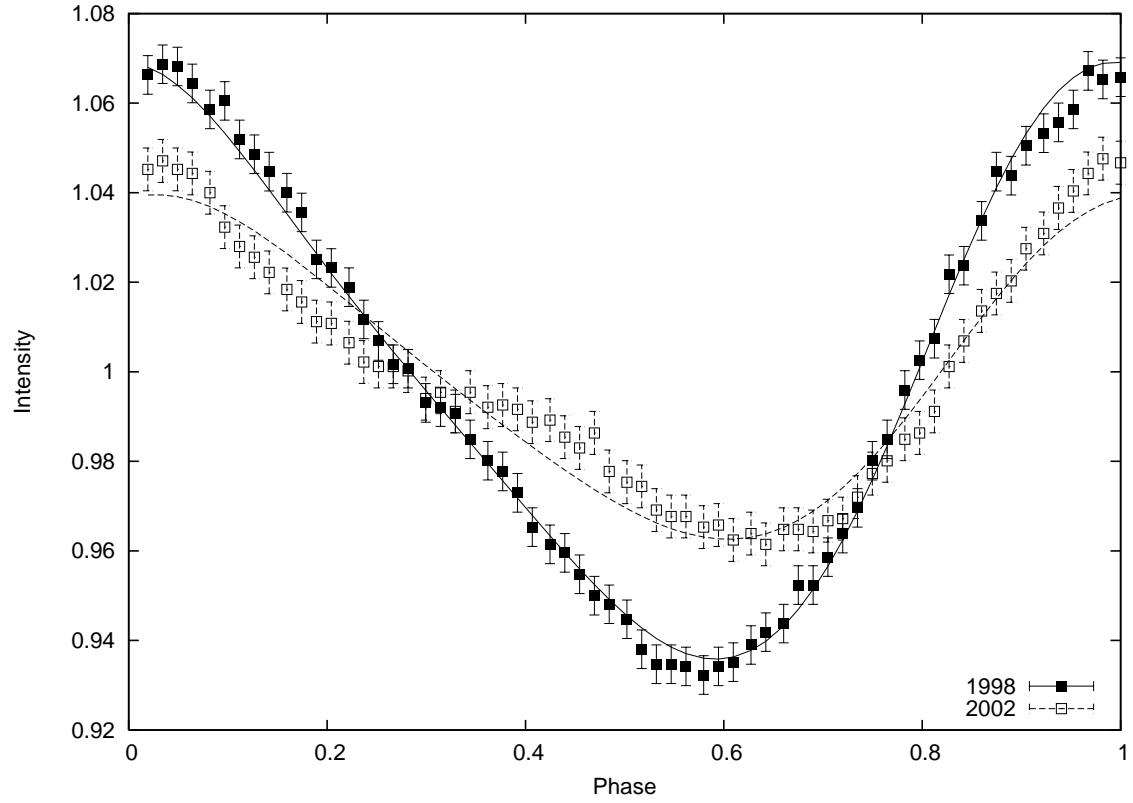


FIG. 1.— Data and best fit models for SAX J1808.4-3658 . The best fit model corresponds to the $2M/R = 0.4$ model presented in Table 4. Data points are from Papitto et al. (2005).

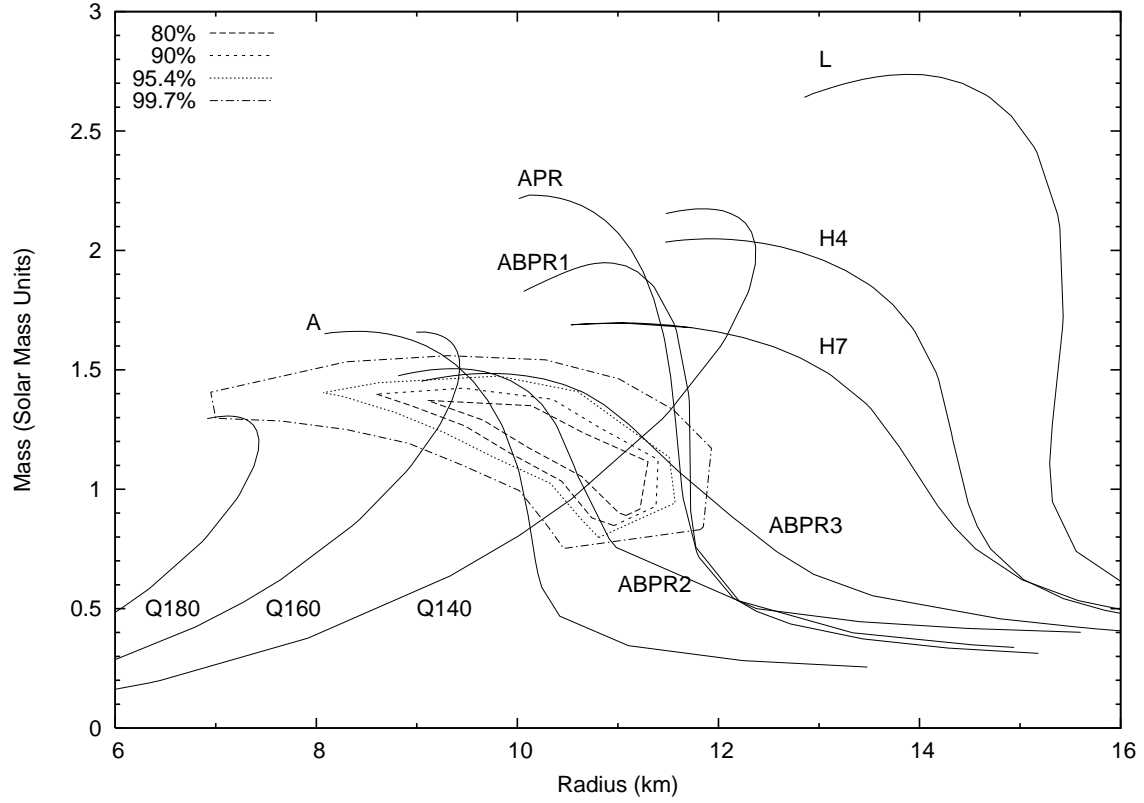


FIG. 2.— Mass versus radius curves for compact stars rotating at 401 Hz. Confidence contours corresponding to 80%, 90%, 95.4% and 99.7% are plotted as dashed curves. The EOS plotted are: A (Arnett & Bowers 1977), ABPR1-3 (mixed quark and hadron phase) (Alford et al. 2005), APR (Akmal et al. 1998), H4 & H7 (hyperons) (Lackey, Nayyar, & Owen 2006), L (Arnett & Bowers 1977), and quark stars denoted Q140-Q180 (where the number corresponds to the value of the bag constant in MeV/fm^3) (Glendenning 2000).